SRTTU
Journal of Computational and Applied Research in Mechanical Engineering
jcarme.sru.ac.ir
JCARME
ISSN: 2228-7922

Research paper

Comparison of conditional scalar dissipation rate models on simulation of pilot stabilized methanol flame

M. Zakyani[a,*]

[a]*Aerospace Research Institute (ARI), Tehran, 1465774111, Iran*

Article info:

Article history:

Received: 00/00/0000
Accepted: 00/00/0018
Revised: 00/00/0000
Online: 00/00/0000

Keywords:

Turbulent combustion modeling,
Amplitude mapping closure,
Conditional volume averaging,
Pollution emission.

***Corresponding author:**
zakyani@ari.ac.ir

Abstract

The paper presents Large Eddy Simulation (LES) Conditional Moment Closure (CMC) simulation of pilot stabilized methanol flame to study the effects of Conditional Scalar Dissipation Rate (CSDR). Two models are used in this research to evaluate CSDR: Conditional Volume Averaging (CVA) and Amplitude Mapping Closure (AMC). For the turbulence modelling, the dynamic Smagorinsky approach was adopted to allow for local adjustment of Smagorinsky constant. For turbulent combustion modelling, CMC is used. Conditional volume averaging is adopted for calculation of conditional velocity. The temperature, mixture fraction, and major species mass fraction are compared against experimental data along radial direction for both cases. The comparison showed reasonable agreement with the experimental measurements for the temperature. It is also observed that the AMC model is superior in predictions compared to CVA method. Additionally, carbon monoxide and carbon dioxide are predicted with remarkable accuracy. Moreover, the conditional temperature also is in good agreement with experimental data that shows CMC model capabilities in turbulent combustion modelling.

1. Introduction

In the first two decades of the current century, large eddy simulations (LES) have emerged as a promising approach for simulating turbulent combustion problems. By resolving the large energy-containing turbulent scales directly and modeling only the small scales, LES can provide more accurate results than Reynolds-averaged Navier-Stokes (RANS) simulations. However, LES for turbulent reacting flows similar to RANS approach poses several challenges due to the wide range of scales involved. LES has the potential to provide more accurate simulations of turbulent reacting flows compared to RANS methods due to its ability to resolve important turbulent scales [1].

The concepts of flame structure in flamelet model that is frequently used in combustion simulations have certain limitations. Models based on the laminar flamelet hypothesis are often not valid for practical conditions where extinction and re-ignition happen [2]. For non-premixed flames, conditional moment closure

(CMC) originally proposed by [3] and transported probability density function (PDF) methods proposed by [4] show promise for reliable predictions of turbulent flames. However, PDF methods are computationally expensive and therefore their usage is limited.

On the other hand, CMC which is a computationally feasible method, arises as a prominent approach for simulating turbulent combustion. Given mentioned advantages for LES in simulation of turbulent combustion process, it is well-suited for simulating turbulent flames with significant unsteady features. CMC has been successful in predicting single-phase gaseous combustion [5].

Turbulent combustion simulations can be sensitive to the specific model employed for scalar dissipation rate (SDR), this parameter is indeed critical in combustion modeling, as it governs the mixing between fuel and oxidizer molecules [6]. The SDR plays a pivotal role in determining reaction rates and flame stability, underscoring its importance in accurately predicting turbulent reacting flows.

However, in CMC methods, a crucial component is the conditional scalar dissipation rate (CSDR). This quantity represents the average rate at which turbulence mixes a specific scalar field (e.g., temperature or species concentration) within a given mixture fraction sample space. As mentioned, turbulent mixing processes involve non-linear interactions between different scales of motion, which can lead to complex behavior in the conditional scalar dissipation rate.

To overcome these challenges, researchers have developed various closure models for the conditional scalar dissipation rate, such as those based on PDF methods [7], or the presumed mapping function model (PMF) [8]. However, these model are computationally expensive and therfore their usage is limited.

Fox [9] investigates the differences between two models for the CSDR in binary scalar mixing: the beta distribution and the amplitude mapping closure (AMC). It examines whether the improved accuracy of the AMC model justifies its higher computational cost, with a focus on accurately modeling molecular mixing and its effect on the evolution of a passive scalar's PDF in turbulent non-premixed combustion scenarios.

To model CSDR in turbulent spray flames, Wang et al. [10] used artificial neural networks (ANNs) to improve the predictions of dissipation rates in turbulent spray flames by effectively capturing complex, non-linear relationships between input parameters and the conditional scalar dissipation rate.

Amzin and Domagala [11] proposes a mathematical closure for the conditional mean scalar dissipation rate in turbulent premixed combustion. The accuracy of the model is tested against two different Direct Numerical Simulation (DNS) databases. The study reviews the turbulent premixed flames and then proceeds with the modeling of the conditional scalar dissipation rate. The progress variable, which measures the reaction progress in premixed combustion, is defined using temperature or fuel mass fraction. The marginal PDF for the progress variable is determined either by solving transport equations or by presuming a PDF shape. The study provides the mathematical equations and definitions necessary for modeling the scalar dissipation rate.

In this study two CSDR models are used that share both simplicity and accuracy. The first model is conditional volume averaging (CVA) of [12], which is more a method than a model, and the second one is amplitude mapping closure (AMC) model of [13].

Methanol as an alternate fuel exhibits higher octane number in comparison to gasoline, but it possesses a notably lower cetane number than diesel fuel. Furthermore, its flammability limit is leaner than that of both gasoline and diesel oil. As a result of this capability for lean combustion, blends of methanol fuel result in reduced emissions of carbon monoxide (CO) [14].

In response to stringent air pollution regulations and the potential of biofuel as an alternative, this study investigates the combustion of methanol as a biofuel. Specifically, the combustion of non-premixed pre-vaporized methanol is studied. The flame stabilization is achieved through a pilot, and experimental measurements were conducted at the combustion test facility located at the University of Sydney [14].

Finally, the results are compared against experimental measurements of [14] and numerical simulation of [15] which is a RANS-PDF modeling of the flame.

2. Flow modeling

Applying Favre filter to the Navier-Stokes equations, the final equation reads

$$\frac{\partial \overline{\rho}}{\partial t}+\frac{\partial \overline{\rho}\tilde{u}_i}{\partial x_i}=0 \quad (1)$$

$$\frac{\partial \overline{\rho}\tilde{u}_i}{\partial t}+\frac{\partial \overline{\rho}\tilde{u}_i\tilde{u}_j}{\partial x_j}=-\frac{\partial \overline{p}}{\partial x_i}+\frac{\partial}{\partial x_j}[\overline{\mu}(\frac{\partial \tilde{u}_i}{\partial x_j}+\frac{\partial \tilde{u}_j}{\partial x_i}-\frac{2}{3}\delta_{ij}\frac{\partial \tilde{u}_k}{\partial x_k})-\tau_{ij}^{sgs}] \quad (2)$$

The Favre filtered mixture fraction equation is given by

$$\frac{\partial \overline{\rho}\tilde{z}}{\partial t}+\frac{\partial \overline{\rho}\tilde{u}_i\tilde{z}}{\partial x_i}=\frac{\partial}{\partial x_i}(\overline{\rho}(\overline{D}_z+D_t)\frac{\partial \tilde{z}}{\partial x_i}) \quad (3)$$

The sub-grid scale (SGS) stress term in the Favre filtered momentum equations can be modeled as

$$\tau_{ij}^{sgs}-\frac{1}{3}\tau_{kk}^{sgs}\delta_{ij}-2\mu_t(\tilde{S}_{ij}\frac{1}{3}\tilde{S}_{mm}\delta_{ij}) \quad (4)$$

In the equation mentioned above, our objective is to determine the turbulent viscosity, denoted as μ_t. Various approaches have been put forth to define turbulent viscosity on the sub-grid scale. An early model known as the Constant Smagorinsky model was introduced to compute the sub-grid scale component of the momentum equations [16]. According to Smagorinsky's proposition, the turbulent diffusivity can be evaluated as follows:

$$\mu_t=\overline{\rho}(C_S\Delta)^2|\tilde{S}_{ij}| \quad (5)$$

$$|\tilde{S}_{ij}|=\sqrt{2\tilde{S}_{ij}\tilde{S}_{ij}} \quad (6)$$

Here, C_S represents the Smagorinsky constant, and Δ signifies the filter width, which is determined by the cubic root of the volume of the local grid cell.

A challenge associated with the constant Smagorinsky model is the need to finely adjust the Smagorinsky constant for each simulation scenario. To address this concern, the dynamic approach introduced by [17] offers a solution by adopting the inherent scale similarity in turbulent fluid motion to dynamically tailor the Smagorinsky constant at a local level.

The sub-grid scale diffusivity in the Favre filtered mixture fraction equation is calculated based on the turbulent viscosity and sub-grid scale Schmidt number from

$$D_t=\frac{\nu_t}{Sc_t} \quad (7)$$

Reference [18] propose to use 0.75 for the turbulent Schmidt number. However, 0.7 is assumed for the turbulent Schmidt number in this work. Detail of the numerical algorithms is given in [19].

3. Combustion modeling

In this study, the CMC model is employed to simulate the interplay between turbulence and chemistry. Within the framework of the CMC model, transport equations for conditional species mass fractions and conditional temperature are solved across time, physical space, and mixture fraction space. The resulting equations for conditional species mass fractions and conditional temperature, as outlined by [12], can be expressed as follows:

$$\frac{\partial \widetilde{Y_\alpha|\eta}}{\partial t}+\widetilde{u_i|\eta}\frac{\partial \widetilde{Y_\alpha|\eta}}{\partial x_i}=\frac{\widetilde{\chi|\eta}}{2}\frac{\partial^2 \widetilde{Y_\alpha|\eta}}{\partial \eta^2}+\frac{\partial}{\partial x_i}(\widetilde{D_t|\eta}\frac{\partial \widetilde{Y_\alpha|\eta}}{\partial x_i})+\widetilde{W_\alpha|\eta} \quad (8)$$

$$\frac{\partial \widetilde{T|\eta}}{\partial t}+\widetilde{u_i|\eta}\frac{\partial \widetilde{T|\eta}}{\partial x_i}=\frac{\widetilde{\chi|\eta}}{2}\frac{\partial^2 \widetilde{T|\eta}}{\partial \eta^2}+\frac{\partial}{\partial x_i}(\widetilde{D_t|\eta}\frac{\partial \widetilde{T|\eta}}{\partial x_i})+\frac{\widetilde{\chi|\eta}}{2}[\frac{1}{\widetilde{c_p|\eta}}(\frac{\partial \widetilde{c_p|\eta}}{\partial \eta}+\sum_{\alpha=1}^{n}(c_p)_\alpha\frac{\partial \widetilde{Y_\alpha|\eta}}{\partial \eta})]\frac{\partial \widetilde{T|\eta}}{\partial \eta}+\frac{1}{\widetilde{c_p|\eta}}\frac{1}{\rho}\widetilde{\frac{\partial p}{\partial t}|\eta}+\frac{\widetilde{W_T|\eta}}{\widetilde{c_p|\eta}} \quad (9)$$

where $\widetilde{Y_\alpha|\eta}$ stands for the Favre conditional filtered mass fraction of species α and $\widetilde{T|\eta}$ stands for the Favre conditional filtered temperature. The contribution associated with pressure's temporal changes in the conditional temperature equation is disregarded due to the implementation of a low Mach approximation in this study. The determination of unconditional mass fractions and temperature involves integrating the conditional values, obtained by solving the conditional equations, with the FDF (Filtered Density Function).

$$\tilde{\varphi} = \int \widetilde{\varphi|\eta}\tilde{P}(\eta)d\eta \quad (12)$$

As FDF a β-function is used whose shape depends on the first and the second moment of the mixture fraction. The first moment is the filtered mixture fraction for which a transport equation is solved at every iteration. The second moment is the sub-grid scale variance of the mixture fraction. To find the mixture fraction variance a local equilibrium assumption is used

$$\widetilde{z''^2} = C\Delta^2|\nabla\tilde{z}|^2 \quad (13)$$

A value equals to 0.09 for C is chosen following [18].

Modeling conditional scalar dissipation rate, $\widetilde{\chi|\eta}$, conditional velocitie, $\widetilde{u_i|\eta}$, and conditional turbulent diffusion, $\widetilde{D_t|\eta}$, are very important in the CMC model acording to [3]. For the calculation of conditional velocity and conditional turbulent diffusion, the LES data is subjected to conditional volume averaging following [12]. Details of the calculation procdure is given in [20]. Details of calculation of the conditional scalar dissipation rate is given in below.

3.1. Modeling condistional scalar dissipation rate (CSDR)

In turbulent combustion, the scalar dissipation rate (SDR) is a measure of how quickly a scalar field (e.g., temperature, species concentration, or mixture fraction) is being mixed by turbulence. The SDR represents the rate at which turbulent fluctuations are mixing the scalar field. In other words, it measures how quickly the scalar is being stirred by turbulence.

In current study, the scalar dissipation rate is obtained using a simple equilibrium model.

$$\tilde{\chi} = 2\left(\frac{\tilde{\mu}}{Sc} + \frac{\mu_t}{Sc_t}\right)|\nabla\tilde{z}|^2 \quad (14)$$

where Sc is laminar Schmidt numbers which is 0.7 in this work and $\tilde{\mu}$ is filtered dynamic viscosity.

As mentined eraliear, two models are used for the calculation of the conditional scalar dissipation rate. In the first model, similar to the model used for conditional velocity and conditional turbulent diffusion, the LES data is subjected to conditional volume averaging (CVA) following [12]. The second model is the amplitude mapping closure (AMC) where is given according to [21]:

$$\widetilde{\chi|\eta} = \chi_0\, G(\eta) \quad (15)$$

where

$$G(\eta) = exp\{-2[erf^{-1}(2\eta - 2)]^2\} \quad (16)$$

$$\chi_0 = \frac{\tilde{\chi}}{\int_0^1 G(\eta)\tilde{P}(\eta)d\eta} \quad (17)$$

4. Test case description

A piloted burner was developed at the University of Sydney specifically for investigating methanol as well as methane diffusion flames [14]. The setup features an axisymmetric jet comprising a nozzle diameter of $D_j = 7.2\ mm$ and an annulus pilot diameter of $D_p = 18\ mm$. The pilot burner's high-temperature gases stabilize the main flame adjacent to the nozzle.

Prior to entering the burner, the methanol is vaporized within a water bath maintained at approximately 373 K by a set of heating elements. To regulate this exit temperature at 373 K, a feedback controller adjusts three heating elements encircling the central fuel tube. Methanol vapor is discharged from the nozzle at atmospheric pressure, and the burner is aligned within a stream of co-flowing air at 300 K.

The velocity of the burned pilot gas, denoted as u_{pb}, is derived using the unburned pilot gas velocity, u_{pu}, resulting in the relationship $u_{pb} = 6.95 \times u_{pu}$.

Although initial conditions are unmeasured, it can be assumed that laminar flow prevails at the pilot gases' exit plane, while fully developed turbulent pipe flow characterizes the central fuel jet. Schematic of the experimental set up for the Sydney piloted methanol flame is shown in Fig. 1.

The fuel jet velocity is, $u_j = 90.3\ m/s$. Pilot unburned velocity is, $u_{pu} = 3.0\ m/s$ and the coflow air velocity is, $u_c = 15.0\ m/s$. The stoichiometric mixture fraction based on Bilger's formula is equal to 0.135.

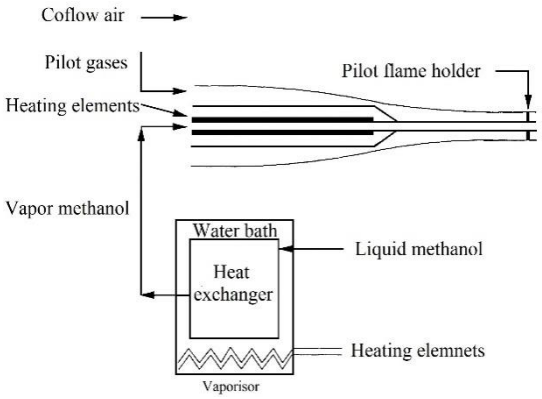

Fig. 1. Schematic picture of Sydney piloted methanol burner experimental setup from [14]

5. Computational setup

For the simulation of the Sydney piloted methanol burner, a cubic domain with $60D_j \times 16D_j \times 16D_j$ is used. The computational cubic mesh consists of $256 \times 96 \times 96$ cells with clustering in axial and lateral directions near the jet region. Ultimately, the mesh is divided into 8 blocks in the axial direction for parallel computations. The mesh is presented in Fig. 2.
A Dirichlet boundary condition is applied at the lateral boundaries, setting the velocity to the co-flow value due to their sufficient distance from the reacting jet's influence. Pressure is imposed at the outflow and interpolated at the inlet, as the simulation employs an incompressible variable density solver. In the lateral direction, the pressure gradient normal to the boundary is set to zero, as no significant pressure variation is expected in that direction. The mixture fraction is set to 1 at the fuel inlet, 0.135 at the pilot stream, corresponding to the stoichiometric mixture fraction of the studied flame, and 0 at the air co-flow inlet. Fuel composition is defined within the mixture fraction space in the CMC code.

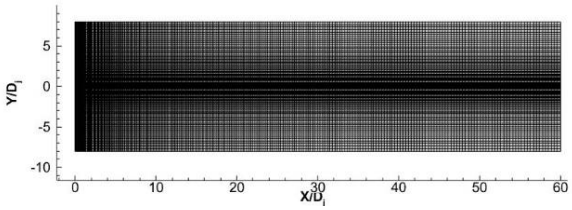

Fig. 2. Mesh cross section in jet center plane for Sydney piloted methanol burner simulation

6. Results and discussion

The contour plot depicted in Fig. 3 for both instantaneous and time-averaged temperature fields, validating the use of Dirichlet boundary conditions due to the flame's sufficient distance from lateral boundaries. Elevated temperatures are observed near the pilot stream due to the premixed inflow of C_2H_2, H_2, CO_2, and air. The instantaneous temperature field reveals a highly turbulent jet with interspersed hot and cold regions, indicating significant mixing between fuel and air.
Localized hot spots in the instantaneous field correspond to intense combustion areas, reflecting the unsteady, intermittent behavior of the turbulent flame. These fluctuations are most prominent in the upstream regions near the jet exit, where mixing layer instabilities create small-scale structures contributing to the flame's transient nature. This turbulent behavior highlights the dynamic nature of combustion in this region.
In contrast, the time-averaged temperature field exhibits a smoother, more symmetric distribution, showing the flame's statistical stability over time. The high-temperature core extends downstream, gradually widening as fuel mixes with air and temperature decays. The clear separation between the hot jet core and the cooler surrounding flow confirms the presence of a stable flame structure, even amidst the turbulence observed in the instantaneous field.

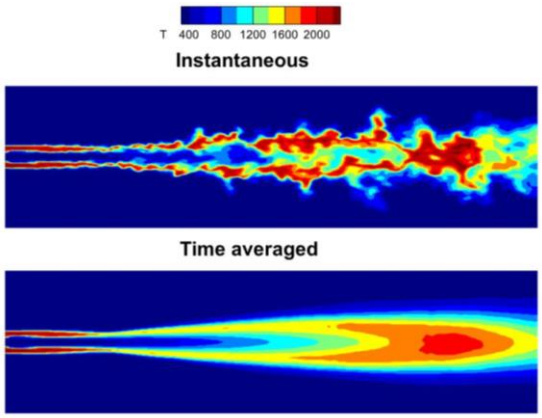

Fig. 3. Instantaneous and time averaged temperature contour plot

The results for two different CSDR i.e., CVA and AMC, models are compared against available experimental data of [14] and numerical results of [15]. Fig. 4 offers a comparative visual representation of the temperature across the radial direction. The analysis is confined to a few points of interest given in the experimental dataset, as indicated within the illustration.

At x=72 mm, the red solid curve (CVA results) and the green dashed curve (AMC results), which both represents the current results, closely follows the trend of the experimental data throughout most of the graph. The high and low temperature readings appear to align well between the LES-CMC predictions and the experimental results, with only minor discrepancies.

The comparison between the AMC results, the CVA results and the blue dash dot curve (Sion and Chen results) reveals some discrepancies. While there may be certain regions where the AMC and [15] results closely match, especially at lower radial distances near the jet centerline, overall, significant deviations are seen. In fact, [15] results tend to deviate more significantly from the accurate predictions of AMC in many areas.

The temperature distribution along a radial distance at x=144mm and x=288mm shows some discrepancies between different models (AMC, CVA, Sion and Chen) compared to experimental measurements. While there are some areas of agreement, particularly farther from the jet centerline, significant deviations occur closer to the centerline. At x=288mm, the CVA model results generally agree better with experimental data than AMC model results, specifically around peak temperatures where AMC underestimates them.

The CMC model effectively captures the overall flame structure and temperature decay, though some discrepancies with experimental data persist due to its limitations in resolving fine-scale turbulence-chemistry interactions. Despite this, the model shows good agreement with experimental time-averaged temperature fields at different axial positions, indicating it accurately predicts the flame's general behavior.

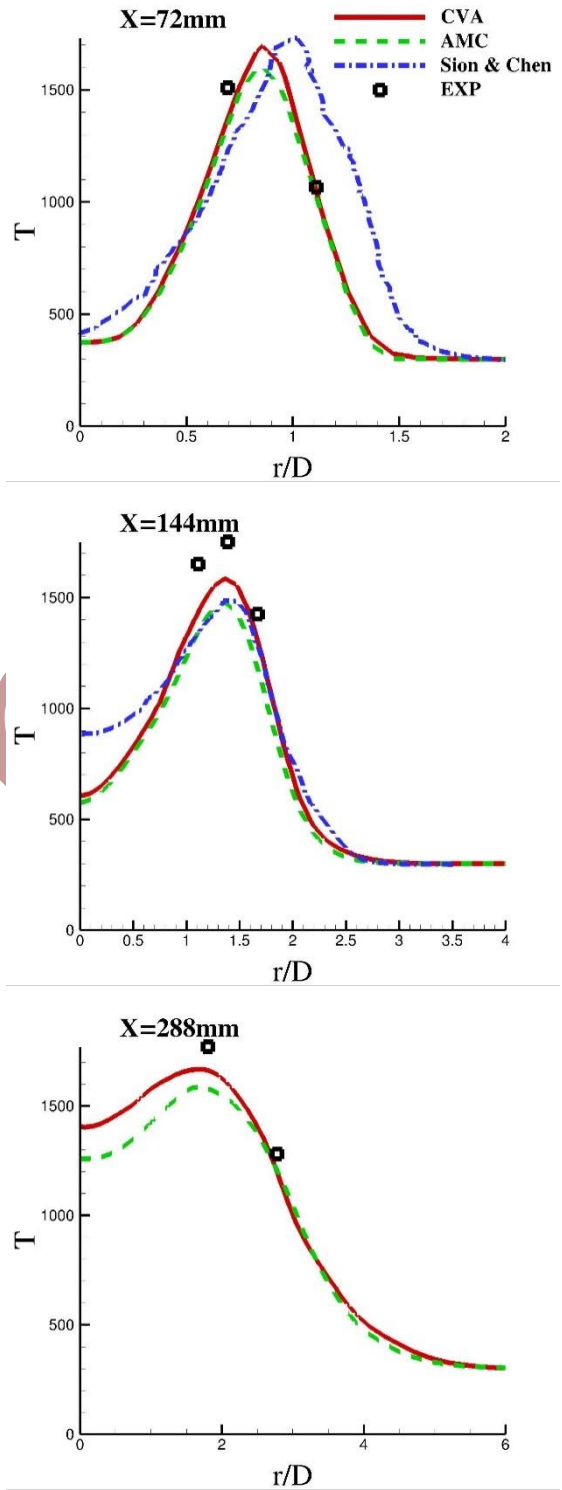

Fig. 4. Comparison of temperature along radial axis against experimental data [14] at x=72 mm (top), x=144 mm (middle) and x=288 mm (bottom)

Fig. 5 provides a visual comparison of mixture fraction along the radial direction, contrasting with the experimental results from [14]. The analysis focuses on specific points of interest, as indicated in the illustration.

At x=72 mm, Both CVA and AMC model displaying excellent agreement with each other as well as experimental results. In fact, this convergence is particularly noteworthy since both models surpass the Sion and Chen numerical results in terms of accuracy.

It is observed that both CSDR models produce identical results at x = 144 mm, similar to what is observed at x=72 mm. In fact, as we approach r/D values less than 1.5, these two models begin to deviate from the experimental measurements. It is worth noting that this deviation occurs relatively close to the centerline (r/D < 1.5), where the flow dynamics are likely to be more complex and sensitive to small variations in the simulation parameters or boundary conditions.

At x=288 mm, both CVA and AMC model produce almost the same mixture fraction distributions across all radial direction. However, around jet centerline AMC model slightly overpredicts mixture fraction. But overall, there is an excellent reproduction of experimental measurements at x = 288 mm.

At the point x=288 mm, both CVA and AMC models exhibit remarkable agreement in their predictions of mixture fraction distributions across all radial directions. In fact, they produce almost identical results, with only minor discrepancies observed.

However, upon closer inspection, it becomes apparent that around the jet centerline, the AMC model slightly overpredicts the mixture fraction values compared to CVA model predictions. This slight deviation is not significant enough to detract from the overall excellent reproduction of experimental data achieved by both models at x=288 mm.

The fact that these two models produce such similar results despite their different approaches highlights the robustness and accuracy of their simulations. The agreement between predicted mixture fraction distributions and experimental measurements further underscores the effectiveness of CVA and AMC models.

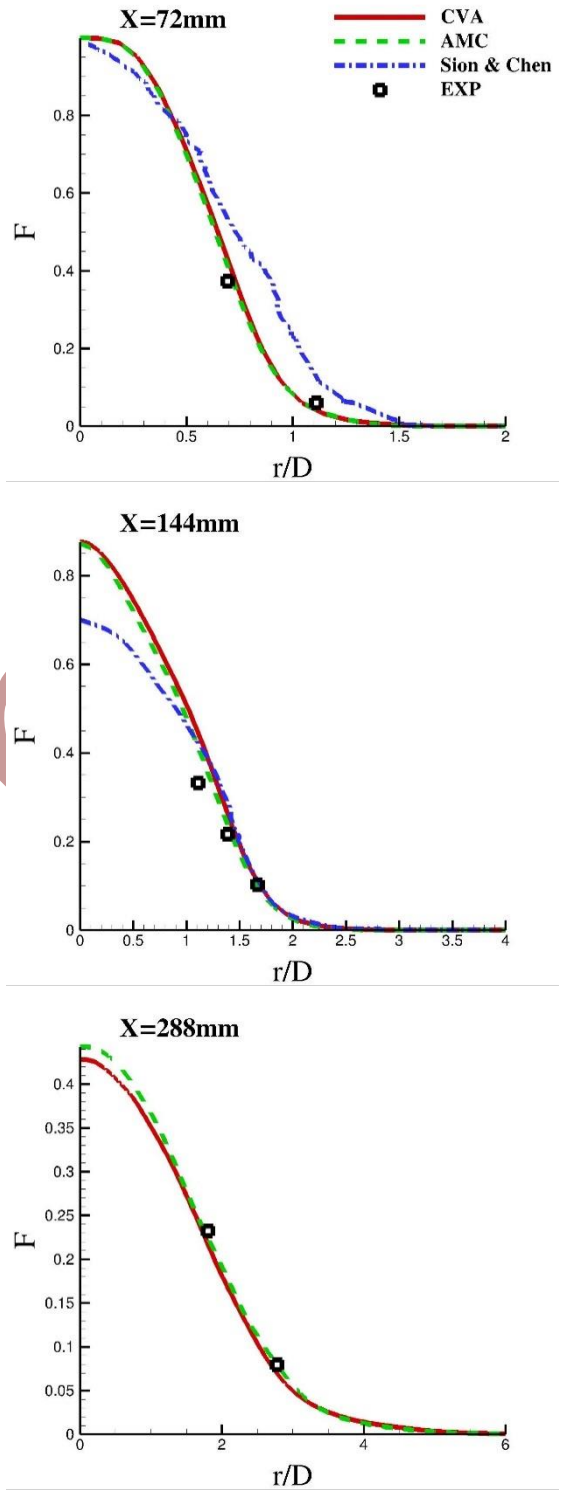

Fig. 5. Comparison of mixture fraction along radial axis against experimental data [14] at x=72 mm (top), x=144 mm (middle) and x=288 mm (bottom)

Fig. 6 presents a visual comparison of the computed carbon dioxide (CO_2) mass fractions across the radial direction with experimental findings from [14]. The analysis is limited to specific points of interest, as indicated within the illustration.

At x = 72 mm, it is evident that the overall trend of the computational model predictions exhibits a high degree of agreement with experimental measurements for both AMC and CVA models. While there may be some overprediction of CO_2 mass fraction at larger radial distances (r/D), the models demonstrate an impressive level of accuracy in capturing the underlying trends. Furthermore, it is clear that both models outperform numerical results obtained by Sion and Chen, highlighting their predictive capabilities.

At x = 144 mm, a notable observation can be made regarding the computational model predictions for carbon dioxide mass fraction. While there may be an overprediction of this parameter, the simulations still closely follow the trends observed in experimental measurements. Moreover, both results demonstrate a level of accuracy superior to those presented by Sion and Chen, underscoring their effectiveness in simulating complex combustion phenomena.

At x = 288 mm, our numerical predictions for carbon dioxide mass fraction align with experimental results for both models. While there may be some slight overestimation when considering radial distances (r/D) near 2, overall agreement between simulations and experiments is observed at this point. It's also worth noting that Sion and Chen did not report carbon dioxide mass fraction measurements at x = 288 mm. Overall, this figure provides valuable insights into the predictive capabilities of these computational models in simulating complex combustion phenomena and highlights their potential for improved accuracy in predicting carbon dioxide distributions within methanol-air mixtures. Moreover, the ability to accurately model CO_2 behavior has significant implications for environmental monitoring and climate change research.

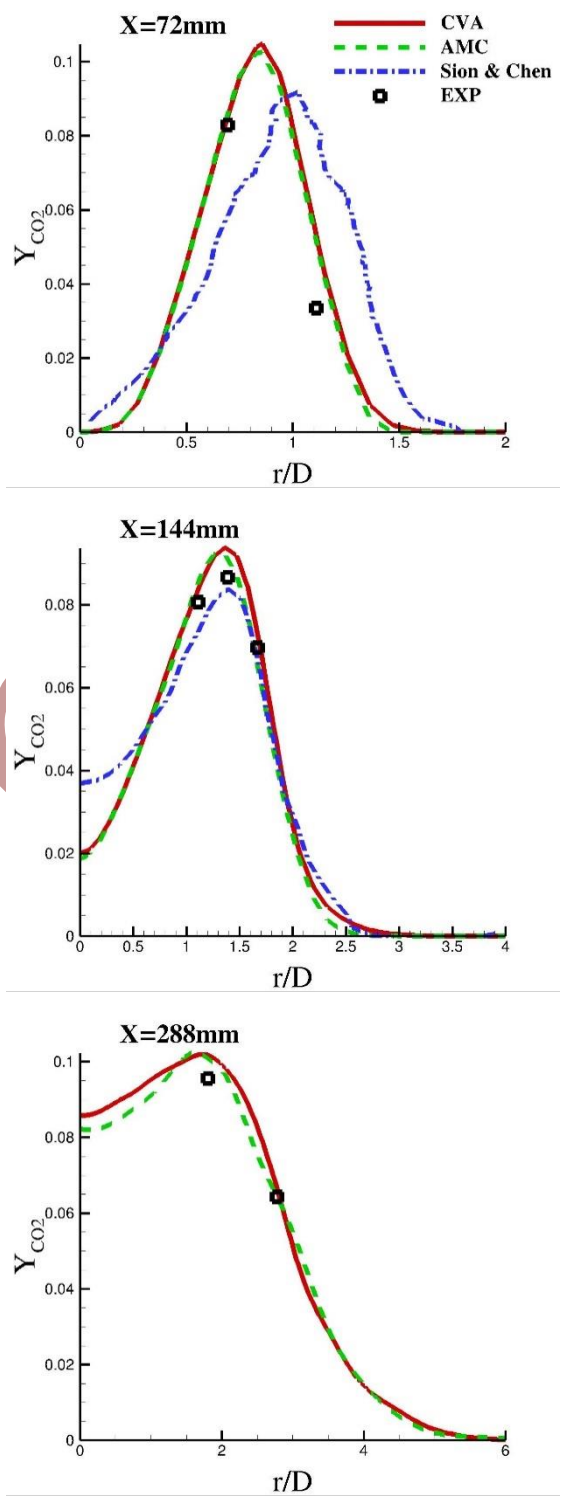

Fig. 6. Comparison of CO_2 (carbon dioxide) mass fraction along radial axis against experimental data [14] at x=72 mm (top), x=144 mm (middle) and x=288 mm (bottom)

Fig. 7 illustrates a visual comparison between the carbon monoxide mass fraction across the radial direction and the experimental results documented in [14]. Again, the analysis is confined to specific points of interest, as indicated within the illustration. As evident from the data, the difference between results for two studies models is more pronounced in carbon monoxide mass fraction prediction.

At x=72 mm, both models follow the trends seen in experimental data. However, AMC model which slightly underpredicts the experiments is in better agreement with experiment than the overpredicted CVA results. Similar to previous graphs, currents results outperform Sion and Chen results.

At x=144 mm, the AMC model gives excellent agreement with experimental data where CVA model largely overpredicts the carbon monoxide mass fraction. For this cross section, Sion and Chen results largely underpredicts the carbon monoxide mass fraction.

At x=288 mm, the CVA results show a slight discrepancy compared to experimental data, with predictions being slightly lower than measurements. In contrast, when comparing CVA results to AMC results, it appears that CVA overpredicts the values obtained from the latter method. Meanwhile, the AMC result itself is underpredicted relative to experimentally measured values. Notably, Sion and Chen's results are not reported for this specific cross-section.

The AMC model demonstrated superior correlation with experimental results relative to the CVA model. Notably, the AMC model exhibited enhanced performance in regions proximal to the fuel nozzle, where the mesh resolution is finer.

Notably, despite differences in CSDR models used, the LES-CMC approach consistently yields more accurate predictions that align closely with experimental data, outperforming the Sion and Chen results. The results demonstrate that the LES-CMC approach can accurately predict pollutant emissions resulting from methanol combustion, making it suitable for practical applications in industry.

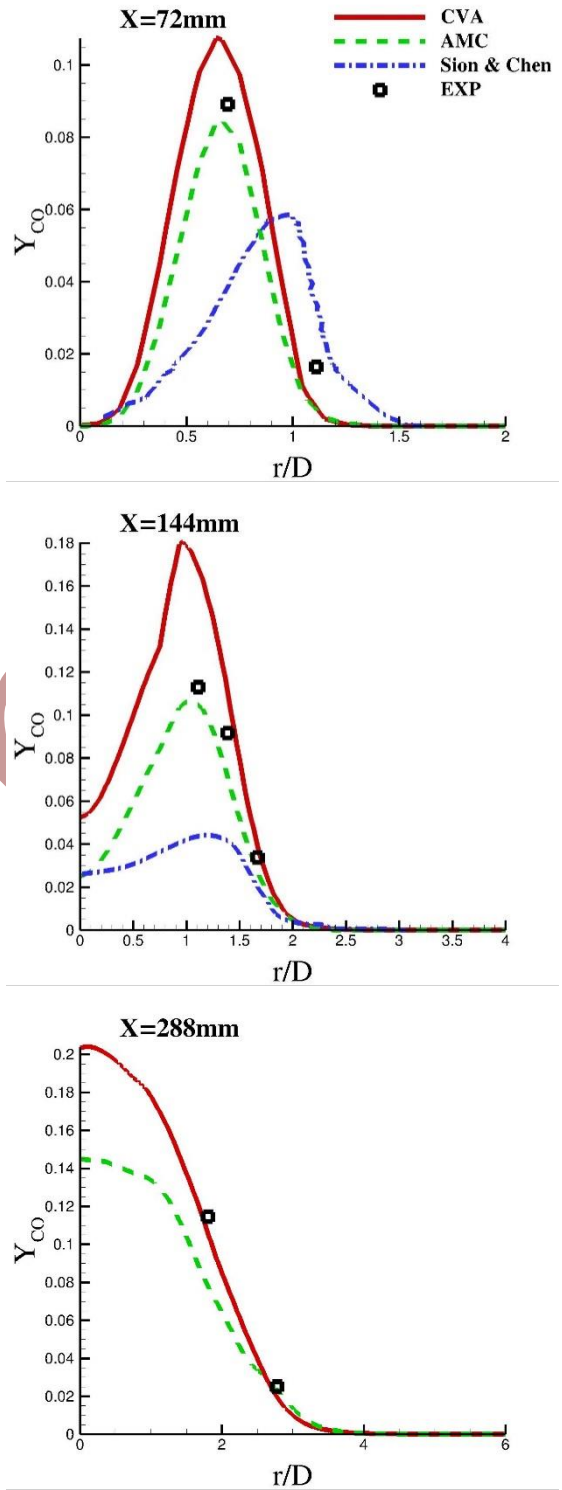

Fig. 7. Comparison of CO (carbon monoxide) mass fraction along radial axis against experimental data [14] at x=72 mm (top), x=144 mm (middle) and x=288 mm (bottom)

7. Conclusions

The present study employs Large Eddy Simulation (LES) combined with Conditional Moment Closure (CMC) to investigate a pilot-stabilized methanol flame, specifically the Sydney piloted methanol flame. The primary objective is to evaluate two distinct models for simulating conditional scalar dissipation rate: Conditional Volume Averaging (CVA) and Amplitude Mapping Closure (AMC). The results obtained from this investigation demonstrate excellent agreement with experimental data, particularly when utilizing the AMC model for species mass fraction.

In addition to its reasonable performance in simulating temperature profiles, the CMC method also demonstrates remarkable accuracy in predicting carbon dioxide (CO_2) and carbon monoxide (CO) emissions within the flame. The alignment between simulation results and experimental data not only validates the reliability of this approach but also underscores its proficiency in capturing essential aspects of pollution emission behavior in this specific flame.

Overall, this study showcases the capabilities of LES-CMC as a powerful tool for simulating complex combustion phenomena, including pilot-stabilized methanol flames. The findings presented here provide valuable insights into the behavior of these types of flames and highlight the potential benefits of using LES-CMC to predict pollution emissions in various industrial settings.

While this study focused on methanol, a well-understood alternative fuel, extending validation to hydrogen and ammonia, both emerging as low-emission fuels, would evaluate the models' ability to predict combustion dynamics under different chemical pathways, especially for emissions like NOx, which are particularly relevant in hydrogen and ammonia combustion.

This expanded validation would also address practical concerns across industries such as automotive, power generation, and aerospace, where different fuel types may be used under varying combustion configurations. By ensuring that the models can accurately predict pollutant formation, flame stability, and efficiency across a range of fuels and flame types, researchers can improve the models' applicability to real-world systems. Moreover, this effort would support the ongoing shift towards alternative and renewable fuels, which is critical for reducing environmental impact and meeting global energy demands.

Acknowledgment

This research was funded by the Aerospace Research Institute (ARI) of the ministry of science, research and technology of the I.R. IRAN. This funding is thankfully acknowledged.

Refrences

[1] H. Pitsch, O. Desjardins, G. Balarac, and M. Ihme, "Large-eddy simulation of turbulent reacting flows", *Progress in Aerospace Sciences*, Vol. 44, No. 6, pp. 466-478, (2008).

[2] H. Pitsch, "Large-eddy simulation of turbulent combustion", *Annual Review of Fluid Mechanics*, Vol. 38, No. 1, pp. 453-482, (2006).

[3] A. Y. Klimenko and R. W. Bilger, "Conditional moment closure for turbulent combustion", *Progress in Energy and Combustion Science*, Vol. 25, No. 6, pp. 595-687, (1999).

[4] S. B. Pope, "PDF methods for turbulent reactive flows", *Progress in Energy and Combustion Science*, Vol. 11, No. 2, pp. 119-192, (1985).

[5] M. Zakyani and C. Lacor, "LES-CMC simulations for piloted non-premixed flames", *Proc. of LES and DNS of ignition processes and complex-structure flames with local extinction*, Poland, pp. 90-97, (2008).

[6] R. W. Bilger, "Some aspects of scalar dissipation", *Flow, Turbulence and Combustion*, Vol. 72, No. 2-4, pp. 93-114, (2004).

[7] C. B. Devaud, R. W. Bilger and T. Liu, "A new method of modeling the conditional scalar dissipation rate", *Physics of*

Fluids, Vol. 16, No. 6, pp. 2004-2011, (2004).

[8] M. Mortensen and B. Andersson, "Presumed mapping functions for eulerian modelling of turbulent mixing", *Flow, Turbulence and Combustion*, Vol. 76, No. 2, pp. 199-219, (2006).

[9] R. O. Fox, "Effect of the conditional scalar dissipation rate in the conditional moment closure", *Physics of Fluids*, Vol. 32, No. 11, (2020).

[10] S. Yao, B. Wang, A. Kronenburg, and O. T. Stein, "Conditional scalar dissipation rate modeling for turbulent spray flames using artificial neural networks", *Proceedings of the Combustion Institute*, Vol. 38, No. 2, pp. 3371-3378, (2021).

[11] S. Amzin and M. Domagała, "Modelling of conditional scalar dissipation rate in turbulent premixed combustion", *Computation*, Vol. 9, No. 3, pp. 26-26, (2021).

[12] S. Navarro-Martinez, A. Kronenburg and F. D. Mare, "Conditional moment closure for large eddy simulations", *Flow, Turbulence and Combustion*, Vol. 75, No. 1-4, pp. 245-274, (2005).

[13] F. Gao and E. E. O'Brien, "A mapping closure for multispecies Fickian diffusion", *Physics of Fluids A: Fluid Dynamics*, Vol. 3, No. 5, pp. 956-959, (1991).

[14] A. R. Masri, R. W. Dibble and R. S. Barlow, "The structure of turbulent nonpremixed flames of methanol over a range of mixing rates", *Combust. Flame*, Vol. 89, No. 2, pp. 167-185, (1992).

[15] M. Sion and J. Y. Chen, "Scalar pdf modeling of turbulent nonpremixed methanol-air flames", *Combust. Sci. Technol.*, Vol. 88, No. 1, pp. 89-114, (1993).

[16] J. Smagorinsky, "General circulation experiments with the primitive equations", *Monthly Weather Review*, Vol. 91, No. 3, pp. 99-164, (1963).

[17] M. Germano, U. Piomelli, P. Moin, and W. H. Cabot, "A dynamic subgrid-scale eddy viscosity model", *Physics of Fluids A: Fluid Dynamics*, Vol. 3, No. 7, pp. 1760-1765, (1991).

[18] N. Branley and W. P. Jones, "Large eddy simulation of a turbulent non-premixed flame", *Combustion and Flame*, Vol. 127, No. 1-2, pp. 1914-1934, (2001).

[19] M. Zakyani, "Large eddy simulation of non-reactive flow in burners", *J. Comput. Appl. Res. Mech. Eng.*, Vol. 12, No. 1, pp. 51-62, (2022).

[20] M. Zakyani, "Numerical study of two reaction mechanisms on delft flame III using large eddy simulation and conditional moment closure approach", *Int. J. Ind. Math*, Vol. 14, No. 3, pp. 339-348, (2022).

[21] P. Gaikwad and S. Sreedhara, "OpenFOAM based conditional moment closure (CMC) model for solving non-premixed turbulent combustion: Integration and validation", *Computers & Fluids*, Vol. 190, pp. 362-373, (2019).